BALNEO RESEARCH Balneo and PRM Research Journal
English Edition
e ISSN 2734 - 8458 p ISSN 2734 - 844X ROMANIAN ASSOCIATION OF BALNEOLOGY

Research article

Human upper limb positional analysis using homogenous transformation matrix

Monica Musunoiu Novetschi [1], Elena Mereuta [1*], Tarek Nazer [1], Daniel Ganea [1] and Claudiu Mereuta [2]

1. "Dunarea de Jos" University of Galati, Faculty of Engineering, Department of Mechanical Engineering; monica.novetschi@ugal.ro; emereuta@ugal.ro; nazer_tarek@yahoo.com; daniel.ganea@ugal.ro
2. "Dunarea de Jos" University of Galati, Faculty of Faculty of Physical Education and Sport, Department of Individual Sports, and Physiotherapy; claudiu.mereuta@ugal.ro

* Correspondence: Elena Mereuta, E-mail: emereuta@ugal.ro

Citation: Novetschi M.M., Mereuta E. and Nazer T., Ganea D., Mereuta C. - Human upper limb positional analysis using homogenous transformation matrix
Balneo and PRM Research Journal **2023**, *14(3): 567*

Academic Editor(s):
Constantin Munteanu

Reviewer Officer:
Viorela Bembea

Production Officer:
Camil Filimon

Received: 05.08.2023
Accepted: 15.08.2023
Published: 01.09.2023

Reviewers:
Mariana Rotariu
Marius Turnea

Abstract: A mathematical model is presented to determine the spatial displacement of an end-effector attached to the human upper limb kinematic chain. The proposed method in-volves the successive application of the homogenous rotation matrices associated with each element movement to determine the general transfer matrix or the so-called homoge-neous transformations matrix. This method is proven to be an error free method for esti-mating the position and orientation of an end-effector attached to a kinematic chain. The methodology presented in this paper combines a well know mathematical technique used in engineering (in the development of space robots) and the anatomical features of the human upper limb to estimate not only the end-effector 3D position but also the limb pos-es during a particular displacement.

Keywords: homogenous transformation, mathematical model, human body, kinematic

1. Introduction

The human body is a complex and optimized mechanism able to perform a wide range of movements. With preponderance, human body kinematic chains produce 3D displacements. This aspect characterizes not only these chains, but the whole body, as spatial mechanisms composed of multitude of heterogenous subsystems. Studies in the field of biomechanics can be oriented to molecular level [1–4], cellular [5–9], organs [10–12], thermodynamics [13–15], fluid mechanics [16–19], material science [20–22], limb kinematic [23–27] and kinetics [28–30] and so on [31]. As can be seen, in the last half of the century, scientists all over the world orientated exponentially their cutting-edge research to human body mechanisms. Thus, mathematical modeling plays a main role in the development of analytical techniques and technologies not only in engineering [32,33] but also in medicine [34–37]. For example, 2D and 3D simulation tools are exclusively running on math models. In biomechanics, as in other fields, researchers all over the world are constantly working to develop the best techniques in the field.

Mathematical models represent the foundation of human body positional, kinematic, and kinetic analysis. Human gait for example apparently is a symmetrical and synchronized action between the left and the right side. However, there is a desynchronization between both sides [38]. This desynchronization changes the kinematic chains laws of motion. The locomotor system asymmetries are transposed to the upper body and especially to the upper limbs that presents a pendulum movement which has the aim of balancing the body. Thus, the human body desynchronization can be evaluated through graphical and non-graphical methods that are based on mathematical modelling.

The main contribution of this research paper is using the homogenous transformations method (HT method) by taking in consideration the connectivity between

joints (number of kinematic elements and degrees of freedom) to improve human motion monitoring accuracy. The basic idea is to use HT method for forward kinematics to calculate human body position during a particular action. More precisely, the 3D position of an end effector attached at the end of the last kinematic element was tracked. HT method uses the relative and absolute positions between joints and kinematic elements. This linkage constraints to some extent limit the drift errors that sensors can have in determining the position vector. Thus, the data provided from such analysis may accurately predict if there is imbalance during biped locomotion by comparing data from symmetrical kinematic chains.

2. Results

The mathematical algorithm presented above was tested in 3 conditions regarding the kinematic chain degrees of freedom (2DoF, 4DoF and 6DoF), ten position each. The DoF of the presented model can be variated by blocking one or multiple joints, respectively movements (θ_i=0). The lengths of the kinematic elements are presented in table 1. These data were measured on a random subject and are input data variables for the mathematical model.

Table 1. Upper limb kinematic elements lengths.

Humerus length (m)	Ulna length (m)	Hand length (m)
0.27	0.29	0.18

2.1. 2DoF kinematic chain

Figure 1 describe the end-effector plane motion in a 2D respectively 3D representation for the 2DoF case (θ_1 and θ_4 from table 2).

The angular ranges of movement after which the kinematic chain was simulated are presented in table 2. According to the resulted data, the end-effector trajectory is generated by the rotational movements of the shoulder and wrist joints along an axis perpendicular to the frontal plane $x_0O_0y_0$. The movement of the effector is related to the origin of the system $O_0x_0y_0z_0$. Thus, the rotational movement along the O_0z_0 (figure 1 b.) axis is described in the plane $x_0O_0y_0$ (figure 1 a.). All 10 successive positions described by the effector are presented in figure 1.

The movement of the effector is described by the increase of the joint parameters followed by the decrease and implicitly the return to the initial state of rest (table 1). The final position (table 1 - Pos.10) is overlapped with the initial one (table 1 - Pos.1) when all joint parameters are equal to 0^O.

In this subchapter the human upper limb and implicitly the end-effector simulates abduction-adduction movement.

Table 2. The variation of the joint parameters for the 10 successive positions described by the end-effector in the 2DoF case.

	Pos. 1 (^{O})	Pos. 2 (^{O})	Pos. 3 (^{O})	Pos. 4 (^{O})	Pos. 5 (^{O})	Pos. 6 (^{O})	Pos. 7 (^{O})	Pos. 8 (^{O})	Pos. 9 (^{O})	Pos. 10 (^{O})
θ_1	0	10	15	20	25	30	40	20	10	0
θ_2	0	0	0	0	0	0	0	0	0	0
θ_3	0	0	0	0	0	0	0	0	0	0
θ_4	0	2,5	5	7,5	10	10	5	5	2,5	0
θ_5	0	0	0	0	0	0	0	0	0	0
θ_6	0	0	0	0	0	0	0	0	0	0

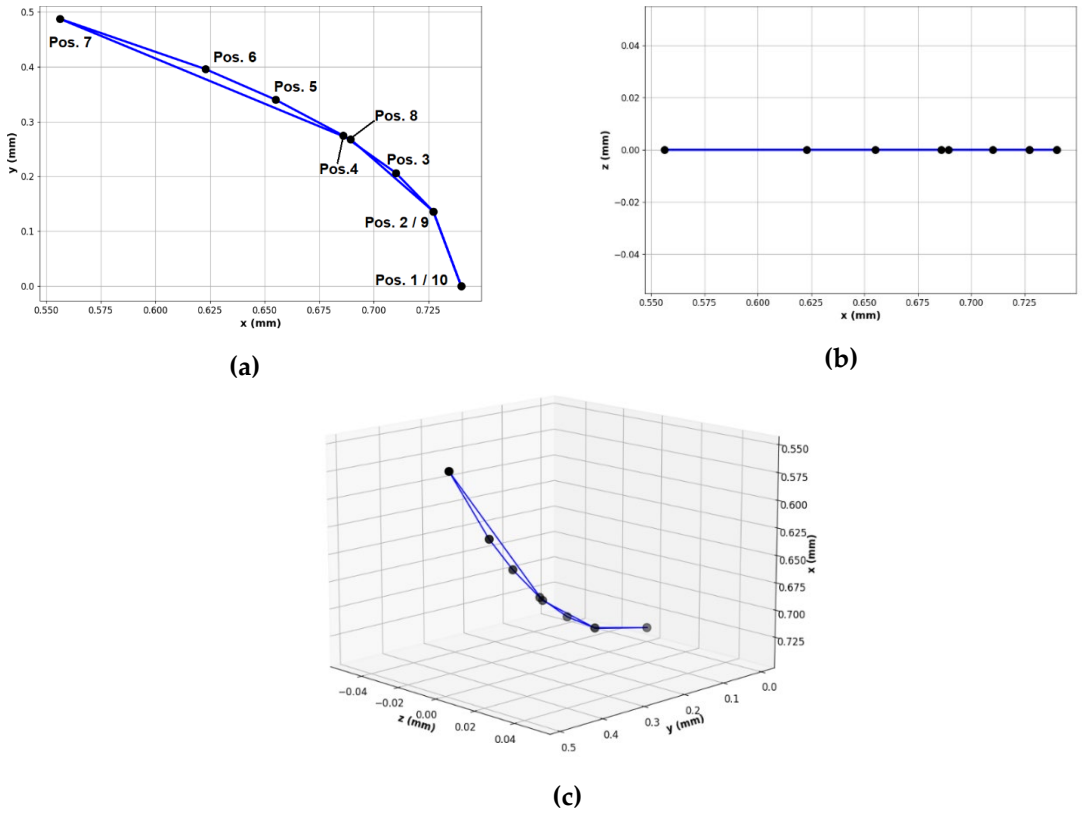

Figure 1. The end-effector trajectory for the 2DoF kinematic chain case: (**a**) xOy trajectory; (**b**) xOz trajectory; (**c**) triortogonal representation Oxyz.

2.2. 4DoF kinematic chain

In this case the kinematic chain of the human upper limb is a plane chain being characterized by 4 degrees of freedom. This implies that 2 degrees of freedom associated with abduction – adduction movement are blocked. According to the trajectory, the end-effector displacement is projected in the sagittal plane ($x_0O_0z_0$). Thus, the trajectory of the end-effector describes flexion-extension movements (all kinematic elements rotate about a perpendicular axis, O_0y_0, on $x_0O_0z_0$ plane). This movement is described in figure 2. Figure 2 represents the result of the upper limb flexion-extension movements in all joints of the kinematic chain (shoulder, elbow, wrist, and fingers). The other possible movements, abduction and adduction, being blocked. Table 3 contains information about the ranges of motion for each joint. In this case only 4 movements are active ($\boldsymbol{\theta_2}$, $\boldsymbol{\theta_3}$, $\boldsymbol{\theta_5}$ and $\boldsymbol{\theta_6}$) and 2 are blocked.

Table 3. The variation of the joint parameters for the 10 successive positions described by the end-effector in the 4DoF case.

	Pos. 1 (°)	Pos. 2 (°)	Pos. 3 (°)	Pos. 4 (°)	Pos. 5 (°)	Pos. 6 (°)	Pos. 7 (°)	Pos. 8 (°)	Pos. 9 (°)	Pos. 10 (°)
$\boldsymbol{\theta_1}$	0	0	0	0	0	0	0	0	0	0
$\boldsymbol{\theta_2}$	0	25	45	55	75	90	45	25	10	0
$\boldsymbol{\theta_3}$	0	20	35	45	90	75	50	25	15	0
$\boldsymbol{\theta_4}$	0	0	0	0	0	0	0	0	0	0
$\boldsymbol{\theta_5}$	0	5	10	15	20	25	20	15	5	0
$\boldsymbol{\theta_6}$	0	1	2	3	4	5	6	3	1	0

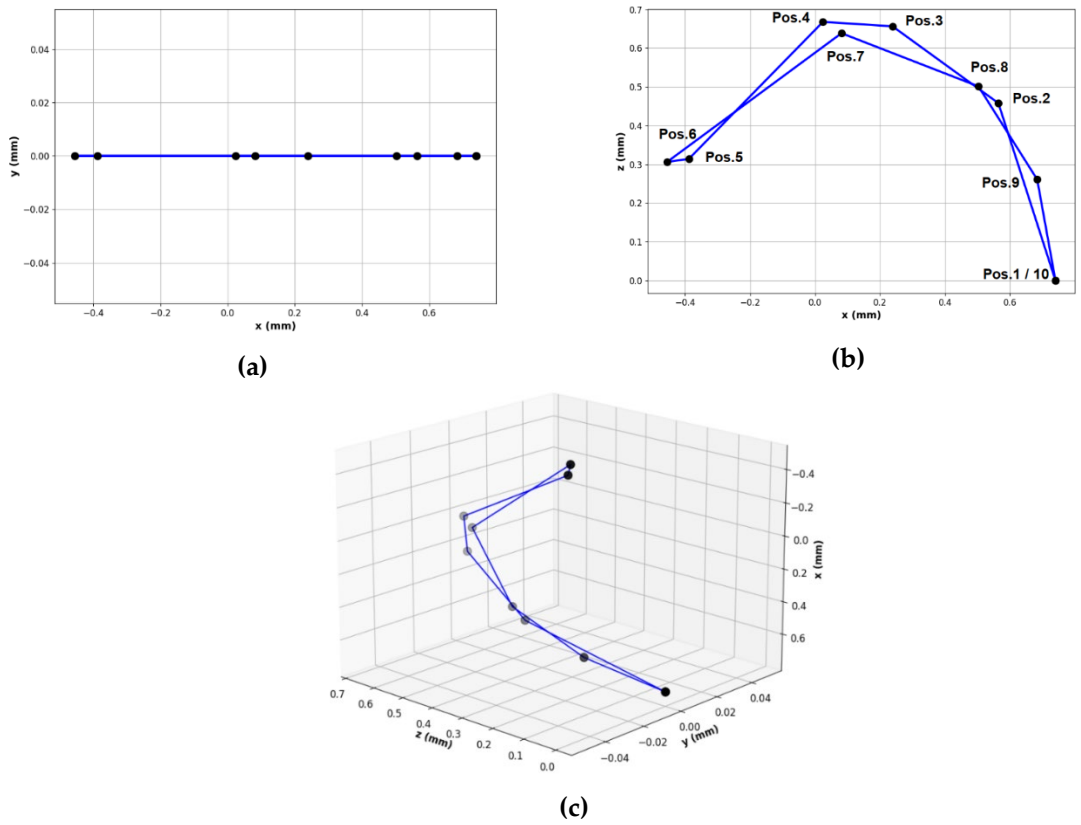

Figure 2 The end-effector trajectory for the 4DoF kinematic chain case: (**a**) xOy trajectory; (**b**) xOz trajectory; (**c**) triortogonal representation Oxyz.

2.3. 6DoF kinematic chain

Compared to the other two cases presented previously, the 6DoF kinematic chain is more complex in terms of displacement. Because all 6 joints (movements) are active (table 4), the end-effector trajectory describe projections in all three reference planes (figure 3). Thus, this kinematic chain is considered a spatial kinematic chain.

Table 4. The variation of the joint parameters for the 10 successive positions described by the end-effector in the 6DoF case.

	Pos. 1 (°)	Pos. 2 (°)	Pos. 3 (°)	Pos. 4 (°)	Pos. 5 (°)	Pos. 6 (°)	Pos. 7 (°)	Pos. 8 (°)	Pos. 9 (°)	Pos. 10 (°)
θ_1	0	10	15	20	25	30	40	20	10	0
θ_2	**0**	25	45	55	75	90	45	25	10	0
θ_3	**0**	20	35	45	90	75	50	25	15	0
θ_4	0	2,5	5	7,5	10	10	5	5	2,5	0
θ_5	**0**	5	10	15	20	25	20	15	5	0
θ_6	**0**	1	2	3	4	5	6	3	1	0

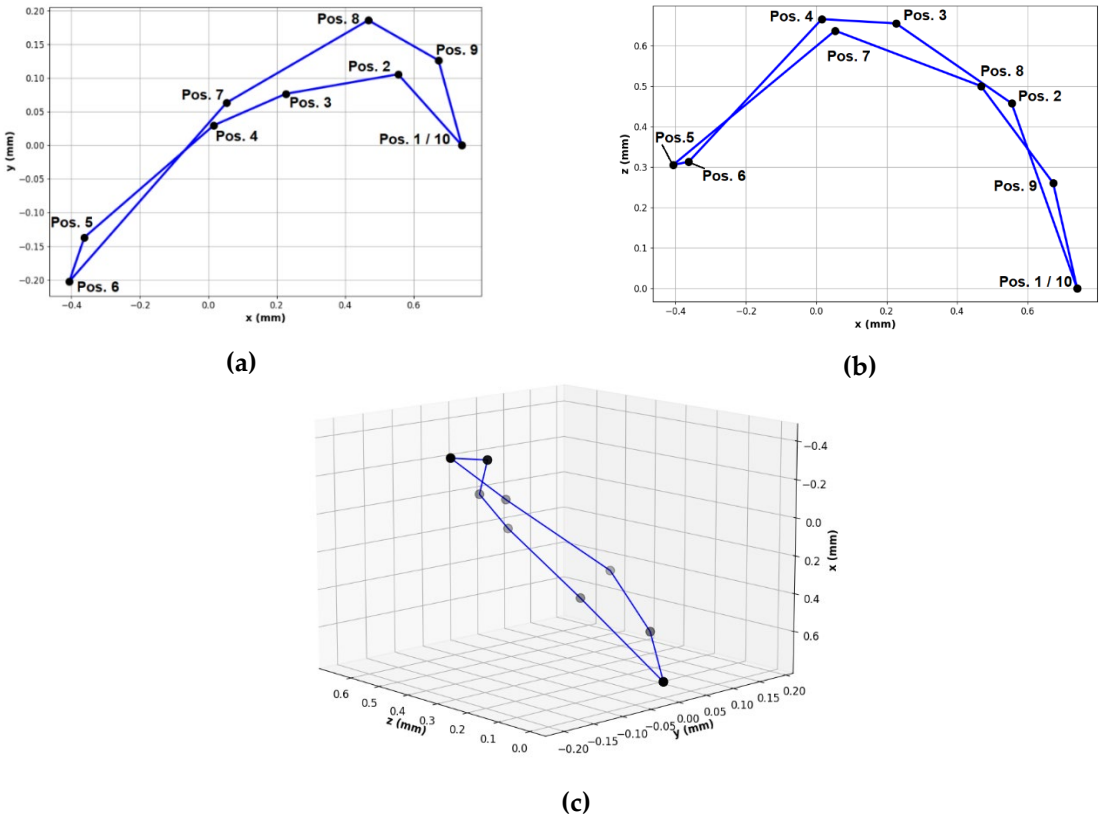

Figure 3. The end-effector trajectory for the 6DoF kinematic chain case: (**a**) xOy trajectory; (**b**) xOz trajectory; (**c**) triortogonal representation Oxyz.

3. Discussion

The displacement of the human body, regardless of the analyzed kinematic chain, is a complex one. Thus, the kinematic chains (lower limbs, upper limbs, trunk, the entire body) can perform planar or spatial movements. So kinematic chains can be planar or spatial. However, rarely the movements produced by the kinematic chains are exclusively planar movements. In this case, only if the aim is to stimulate particular movements such as flexion and extension or abduction and adduction.

The presented model can be adjusted in terms of complexity. It can simulate a planer or a spatial kinematic chain. At this moment the model offers the possibility to simulate a chain with a wide range of degrees of freedom (from 1DoF to 6DoF). However, it can be easily adjusted even to a higher complexity (mode than 6DoF) by adding homogenous transformation matrices for the remained possible movements of the human body upper limb. The maximum complexity to which this model can be adjusted without considering the joints of the phalanges is 10 DoF.

4. Materials and Methods

4.1. Homogenous transformation matrix

The research methodology is presented in a three-stage summarized form according to figure 4. The first stage refers to the input data associated with the mechanical system in question. These data contain information about the length of kinematic elements (table 1), types of kinematic joints and angular ranges of motion (tables 2, 3, and 4). Second, was developed the mathematical models for the direct kinematic analysis using HT method. Thus, the rotation matrices (R_i^{i-1}), the displacement vectors (d_i^{i-1}) and the orientation of the local tri orthogonal axis systems ($O_nx_ny_nz_n \rightarrow O_mx_my_mz_m$) are deduced for each kinematic joint in consideration. Third, a Python script was developed that aims to determine the

HT general matrix that contains information about the displacement vector of the end-effector.

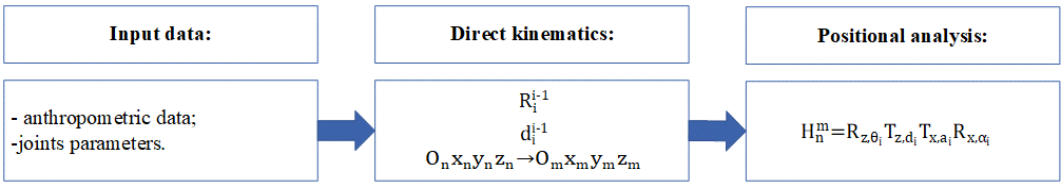

Figure 4. The methodology for determining the position of the effector.

The input data stage refers to kinematic chain modeling that in biomechanics as in machine theory (robotics) requires simplifying assumptions. Thus, the limbs for example are kinematic chains assemblies of non-deformable kinematic elements articulated by simple rotation joints. In the human body there are various types of joints (cylindrical, spherical, translational, etc.). For joints that allow two or three rotations around the reference system simplifying hypothesis is accepted. This assumption requires that any rotation about an axis be considered as a cylindrical joint. The spherical joint (hip joint, shoulder joint) is considered as a superposition of three cylindrical joints. In this case, the rotation axes form a triortogonal system [39].

A body is completely determined in a triortogonal system (direct kinematics) if the position of the origin of the attached local reference system and the directions of its axes with respect to the global reference system are known. Any point of the body is positionally determined if the attached axis system represented by a homogeneous transformation matrix H_n^m is known, where m is the initial (reference) position, and *n* the final one. The H_n^m matrix first three columns form the direction cosines of the directions (R_n^m) while the last column the position vector (d_n^m) [40].

Given that the repositioning of human kinematic chains is based on rotational movements (figure 5), the homogeneous matrix in this case is based on homogeneous rotational transformations. The simple rotation matrices about the axes $O_{i-1}x_{-i}$, $O_{i-1}y_{-i}$ and $O_{i-1}z_{-i}$ respectively are given by equations 1, 2 and 3.

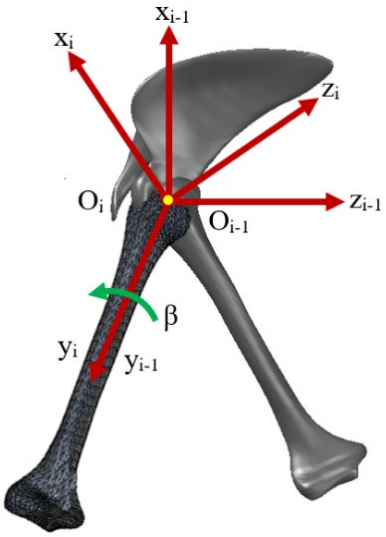

Figure 5. Homogeneous rotational transformation around the Oy axis of the reference system.

$$\begin{bmatrix} x_R \\ y_R \\ z_R \\ 1 \end{bmatrix} = \begin{bmatrix} 1 & 0 & 0 & 0 \\ 0 & \cos\alpha & \sin\alpha & 0 \\ 0 & -\sin\alpha & \cos\alpha & 0 \\ 0 & 0 & 0 & 1 \end{bmatrix} \cdot \begin{bmatrix} x \\ y \\ z \\ 1 \end{bmatrix}, R(\alpha, x_{i-1}) \quad (1)$$

$$\begin{bmatrix} x_R \\ y_R \\ z_R \\ 1 \end{bmatrix} = \begin{bmatrix} \cos\beta & 0 & -\sin\beta & 0 \\ 0 & 1 & 0 & 0 \\ \sin\beta & 0 & \cos\beta & 0 \\ 0 & 0 & 0 & 1 \end{bmatrix} \cdot \begin{bmatrix} x \\ y \\ z \\ 1 \end{bmatrix}, R(\beta, y_{i-1}) \quad (2)$$

$$\begin{bmatrix} x_R \\ y_R \\ z_R \\ 1 \end{bmatrix} = \begin{bmatrix} \cos\theta & \sin\theta & 0 & 0 \\ -\sin\theta & \cos\theta & 0 & 0 \\ 0 & 0 & 1 & 0 \\ 0 & 0 & 0 & 1 \end{bmatrix} \cdot \begin{bmatrix} x \\ y \\ z \\ 1 \end{bmatrix}, R(\theta, z_{i-1}) \quad (3)$$

4.2. Human upper limb kinematic model

In this paper a kinematic model of the upper limb was developed with the respect of the simplifying assumptions and the anatomical considerations presented previously. This model is an open kinematic chain with 6 degrees of freedom that can simulate the anatomical behavior of the human upper limb during biped walking (figure 6).

The shoulder joint and the hand joint are each considered as a superposition of two cylindrical joints. Thus, were associated 2 degrees of freedom to the shoulder joint, 1 degree of freedom to the elbow joint, 2 degrees of freedom to the hand joint, and 1 degree of freedom to the finger joint. Based on this model, the successive positions described by an end-effector positioned on the fingertips were analyzed. Figure 6 show the kinematic model with 6 degrees of freedom. As can be seen, the shoulder and hand joints are represented as overlays of simple rotational joints.

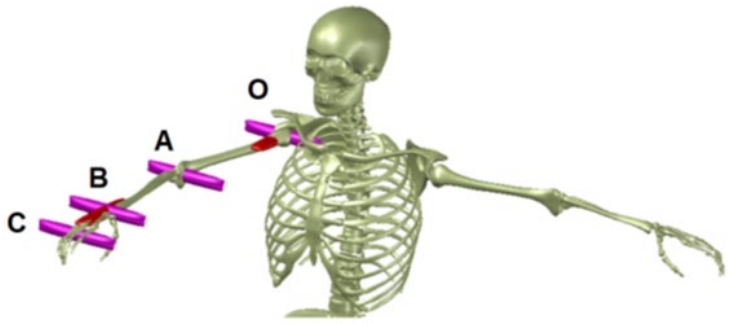

Figure 6. The 6-degree-of-freedom kinematic model of the human upper limb. Point O represents the shoulder joint (origin of the system), point A represents the elbow joint, point B represents the hand joint, and point C represents the finger joint.

Figure 4 illustrates the coordinate systems and the axis orientation of the kinematic chain joints. The anatomical system origin ($O_0x_0y_0z_0$) is in the shoulder joint. The other coordinate systems are positioned in joints having their origins shifted in accordance with the anatomical dimensions of the kinematic elements (table 1). The kinematic elements (skeletal system) are considered in this case as rigid elements. According to homogenous transformation theory, the $O_6x_6y_6z_6$ system copies the orientation of the $O_5x_5y_5z_5$ system and represents the position of the end-effector positioned on the fingertips. The zi axes for $i \in [0,5]$ are the axes associated with the rotational movements generated by kinematic chain joints.

In figure 7 the joints represented with the blue shade produce flexion-extension movements, and those with the green shade abduction-adduction. For this study, was considered as data for the simulation, values in correspondence with those from the previously presented norms. According to specialized literature, the human upper limb is the kinematic chain with the highest degree of mobility.

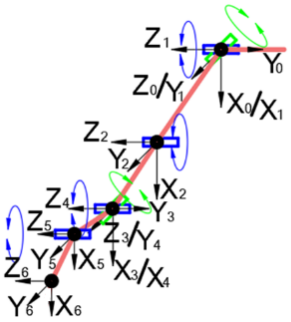

Figure 7. Graphical representation of the joint coordinate systems of the human upper limb 6 degrees of freedom kinematic model and the effector positioned on the fingertips.

4.3. Mathematical modeling of the human upper limb

The configuration of end-effector frame $O_6x_6y_6z_6$ with the respect to the base frame $O_0x_0y_0z_0$ (shoulder joint) is given by the equation 7. The H_6^0 matrix is a matrix product of the 6 homogeneous transformation matrices $(\prod_{i=0}^{6} H_i^{i-1})$.). The general transformation matrix contains information about the displacement vector (d_i^{i-1}) and the rotational matrix (R_i^{i-1}) in a triortogonal system for each joint (movement). The result of the matrix product contains information about plane or spatial displacement of the end-effector. Depending on the complexity, it can contain projections on all planes if the displacement is spatial ($\bar{r}= r_x\bar{i}+r_y\bar{j}+r_z\bar{k}$) or in the plane if it is a parallel plane movement ($\bar{r}= r_x\bar{i}+r_y\bar{j}$ or $\bar{r}= r_x\bar{i}+r_z\bar{k}$).In equation 7, some symbolic notations were made for the trigonometric functions (*c* for *cos* and *s* for *sine*).

$$R_i^{i-1}=R(\theta_i,z_{i-1})\cdot I_i^{i-1} \tag{4}$$

$$d_i^{i-1}=\begin{bmatrix}0\\0\\0\end{bmatrix} \tag{5}$$

$$H_i^{i-1}=\begin{bmatrix} R_i^{i-1} & d_i^{i-1} \\ 0\ \ 0\ \ 0 & 1 \end{bmatrix} \tag{6}$$

$$H_6^0=\prod_{i=0}^{6} H_i^{i-1} = \begin{bmatrix} c\theta_1 & 0 & s\theta_1 & 0 \\ s\theta_1 & 0 & -c\theta_1 & 0 \\ 0 & 1 & 0 & 0 \\ 0 & 0 & 0 & 1 \end{bmatrix} \cdot \begin{bmatrix} c\theta_2 & 0 & -s\theta_2 & l_1\cdot c\theta_2 \\ s\theta_2 & 0 & c\theta_2 & l_1\cdot s\theta_2 \\ 0 & 1 & 0 & 0 \\ 0 & 0 & 0 & 1 \end{bmatrix} \cdot \begin{bmatrix} c\theta_3 & 0 & -s\theta_3 & l_2\cdot c\theta_3 \\ s\theta_3 & 0 & c\theta_3 & l_2\cdot s\theta_3 \\ 0 & -1 & 0 & 0 \\ 0 & 0 & 0 & 1 \end{bmatrix} \cdot \begin{bmatrix} c\theta_4 & 0 & s\theta_4 & 0 \\ s\theta_4 & 0 & -c\theta_4 & 0 \\ 0 & 1 & 0 & 0 \\ 0 & 0 & 0 & 1 \end{bmatrix} \cdot \begin{bmatrix} c\theta_5 & -s\theta_5 & 0 & l_3\cdot 0.5\cdot c\theta_5 \\ s\theta_5 & c\theta_5 & 0 & l_3\cdot 0.5\cdot s\theta_5 \\ 0 & 0 & 1 & 0 \\ 0 & 0 & 0 & 1 \end{bmatrix} \cdot \begin{bmatrix} c\theta_6 & -s\theta_6 & 0 & l_3\cdot 0.5\cdot c\theta_6 \\ s\theta_6 & c\theta_6 & 0 & l_3\cdot 0.5\cdot s\theta_6 \\ 0 & 0 & 1 & 0 \\ 0 & 0 & 0 & 1 \end{bmatrix} \tag{7}$$

5. Conclusions

In this research paper, a novel approach in domain of biomechanics was used to quantify the displacement vector ($\bar{r}= r_x\bar{i}+r_y\bar{j}+r_z\bar{k}$ for 3D movement, and $\bar{r}= r_x\bar{i}+r_y\bar{j}$ or $\bar{r}= r_x\bar{i}+r_z\bar{k}$ for plane displacement) resulting from a positional analysis of the human upper limb. The method approached is that of homogeneous rotation transformations. This method involves determining the rotation matrix and the displacement vector for each joint (movement) studied in relation to the reference joint witch is the global reference system. In this case ($O_0x_0y_0z_0$). The direct result is represented by the scalar components of the displacement vector described by the end-effector. The end-effector is theoretical point located at the tip of the fingers. In table 5 are presented the numerical results of the mathematical model simulation for all 3 cases, 10 positions each.

The mathematical model was developed using the python programming language, which is a fast and efficient language used by researchers all over the world for developing high end solutions.

Table 5. The End-effector displacement vector scalars for all 3 cases.

End-effector position nr.	End-effector displacement vector scalars (2DoF)			End-effector displacement vector scalars (4Dof)			End-effector displacement vector scalars (4Dof)		
	x(m)	y(m)	z(m)	x(m)	y(m)	z(m)	x(m)	y(m)	z(m)
Pos.1	0,740	0,0	0,0	0,740	0,0	0,0	0,740	0,0	0,0
Pos.2	0,727	0,136	0,0	0,564	0,0	0,458	0,554	0,105	0,457
Pos.3	0,710	0,206	0,0	0,238	0,0	0,656	0,225	0,076	0,655
Pos.4	0,685	0,274	0,0	0,024	0,0	0,667	0,015	0,029	0,666
Pos.5	0,654	0,339	0,0	-0,388	0,0	0,313	-0,362	-0,137	0,313
Pos.6	0,622	0,395	0,0	-0,455	0,0	0,306	-0,406	-0,202	0,305
Pos.7	0,556	0,487	0,0	0,081	0,0	0,638	0,053	0,063	0,637
Pos.8	0,689	0,267	0,0	0,502	0,0	0,501	0,467	0,185	0,500
Pos.9	0,727	0,136	0,0	0,683	0,0	0,260	0,671	0,126	0,260
Pos.10	0,740	0,0	0,0	0,740	0,0	0,0	0,740	0,0	0,0

Author Contributions: Conceptualization, E.M. and D.G.; methodology, M.M.N., E.M. and N.T.; software, M.M.N. and D.G.; validation, E.M., C.M. and D.G.; formal analysis, M.M.N.; investigation, N.T.; resources, N.T.; writing—original draft preparation, M.M.N., writing—review and editing, E.M., C.M. and D.G.; visualization, M.M.N. and N.T.; supervision, D.G. and E.M.

Institutional Review Board Statement: Not applicable.

Informed Consent Statement: Not applicable.

Data Availability Statement: Not applicable.

Conflicts of Interest: The authors declare no conflict of interest.

References

1. Kou, S. (Gabriel); Peters, L.; Mucalo, M. Chitosan: A Review of Molecular Structure, Bioactivities and Interactions with the Human Body and Micro-Organisms. *Carbohydrate Polymers* **2022**, *282*, 119132, doi:10.1016/j.carbpol.2022.119132.
2. Malak, D.; Akan, O.B. Molecular Communication Nanonetworks inside Human Body. *Nano Communication Networks* **2012**, *3*, 19–35, doi:10.1016/j.nancom.2011.10.002.
3. Lapenna, D.; Pierdomenico, S.D.; Ciofani, G.; Ucchino, S.; Neri, M.; Giamberardino, M.A.; Cuccurullo, F. Association of Body Iron Stores with Low Molecular Weight Iron and Oxidant Damage of Human Atherosclerotic Plaques. *Free Radical Biology and Medicine* **2007**, *42*, 492–498, doi:10.1016/j.freeradbiomed.2006.11.014.
4. Khan, S.; Katabuchi, H.; Araki, M.; Okamura, H.; Nishimura, R. Molecular Forms of Human Chorionic Gonadotropin in Body Fluids in Gestational Trophoblastic Disease. *Placenta* **1997**, *18*, A9, doi:10.1016/S0143-4004(97)90038-2.
5. Han, B.; Wang, L.; Schotten, H.D. A 3D Human Body Blockage Model for Outdoor Millimeter-Wave Cellular Communication. *Physical Communication* **2017**, *25*, 502–510, doi:10.1016/j.phycom.2017.10.008.
6. Pieri, L.; Chafey, P.; Le Gall, M.; Clary, G.; Melki, R.; Redeker, V. Cellular Response of Human Neuroblastoma Cells to α-Synuclein Fibrils, the Main Constituent of Lewy Bodies. *Biochimica et Biophysica Acta (BBA) - General Subjects* **2016**, *1860*, 8–19, doi:10.1016/j.bbagen.2015.10.007.

7. Görnemann, J.; Hofmann, T.G.; Will, H.; Müller, M. Interaction of Human Papillomavirus Type 16 L2 with Cellular Proteins: Identification of Novel Nuclear Body-Associated Proteins. *Virology* **2002**, *303*, 69–78, doi:10.1006/viro.2002.1670.
8. Tarique, I.; Lu, T.; Tariq, M. Cellular Activity of Autophagy and Multivesicular Bodies in Lens Fiber Cells during Early Lens Development in Rbm24a Mutant of Zebrafish: Ultrastructure Analysis. *Micron* **2023**, *169*, 103446, doi:10.1016/j.micron.2023.103446.
9. Dragoo, J.L.; Shapiro, S.A.; Bradsell, H.; Frank, R.M. The Essential Roles of Human Adipose Tissue: Metabolic, Thermoregulatory, Cellular, and Paracrine Effects. *Journal of Cartilage & Joint Preservation* **2021**, *1*, 100023, doi:10.1016/j.jcjp.2021.100023.
10. Kemėšienė, J.; Rühle, A.; Gomolka, R.; Wurnig, M.C.; Rossi, C.; Boss, A. Advanced Diffusion Imaging of Abdominal Organs in Different Hydration States of the Human Body: Stability of Biomarkers. *Heliyon* **2021**, *7*, e06072, doi:10.1016/j.heliyon.2021.e06072.
11. Cosnier, S.; Le Goff, A.; Holzinger, M. Towards Glucose Biofuel Cells Implanted in Human Body for Powering Artificial Organs: Review. *Electrochemistry Communications* **2014**, *38*, 19–23, doi:10.1016/j.elecom.2013.09.021.
12. Steinbrecht, R.A. The Tuft Organs of the Human Body Louse, Pediculus Humanus Corporis—Cryofixation Study of a Thermo-/ Hygrosensitive Sensillum. *Tissue and Cell* **1994**, *26*, 259–275, doi:10.1016/0040-8166(94)90101-5.
13. Bohlooli, M.; Moosavi-Movahedi, A.A.; Taghavi, F.; Habibi-Rezaei, M.; Seyedarabi, A.; Saboury, A.A.; Ahmad, F. Thermodynamics of a Molten Globule State of Human Serum Albumin by 3-β-Hydroxybutyrate as a Ketone Body. *International Journal of Biological Macromolecules* **2013**, *54*, 258–263, doi:10.1016/j.ijbiomac.2012.12.018.
14. Ndumiso, M.; Buchtová, N.; Husselmann, L.; Mohamed, G.; Klein, A.; Aucamp, M.; Canevet, D.; D'Souza, S.; Maphasa, R.E.; Boury, F.; et al. Comparative Whole Corona Fingerprinting and Protein Adsorption Thermodynamics of PLGA and PCL Nanoparticles in Human Serum. *Colloids and Surfaces B: Biointerfaces* **2020**, *188*, 110816, doi:10.1016/j.colsurfb.2020.110816.
15. Dutta, A.; Chattopadhyay, H. Performance Analysis of Human Respiratory System Based on the Second Law of Thermodynamics. *Journal of Thermal Biology* **2021**, *96*, 102862, doi:10.1016/j.jtherbio.2021.102862.
16. Rajput, S.; Kumar Sharma, P.; Malviya, R. Fluid Mechanics in Circulating Tumour Cells: Role in Metastasis and Treatment Strategies. *Medicine in Drug Discovery* **2023**, 100158, doi:10.1016/j.medidd.2023.100158.
17. Melito, G.M.; Müller, T.S.; Badeli, V.; Ellermann, K.; Brenn, G.; Reinbacher-Köstinger, A. Sensitivity Analysis Study on the Effect of the Fluid Mechanics Assumptions for the Computation of Electrical Conductivity of Flowing Human Blood. *Reliability Engineering & System Safety* **2021**, *213*, 107663, doi:10.1016/j.ress.2021.107663.
18. Dabnichki, P. Unsteady Fluid Mechanics Effects in Water Based Human Locomotion. *Mathematics and Computers in Simulation* **2011**, *82*, 471–482, doi:10.1016/j.matcom.2011.09.005.
19. Burchell, C.; Kourmatzis, A.; Zhao, Y.; Raco, J.; Mekonnen, T.; Chan, H.-K.; Cheng, S. Effects of Respiratory Rate on the Fluid Mechanics of a Reconstructed Upper Airway. *Medical Engineering & Physics* **2022**, *100*, 103746, doi:10.1016/j.medengphy.2021.103746.
20. Gaur, S.; Singh Raman, R.K.; Khanna, A.S. In Vitro Investigation of Biodegradable Polymeric Coating for Corrosion Resistance of Mg-6Zn-Ca Alloy in Simulated Body Fluid. *Materials Science and Engineering: C* **2014**, *42*, 91–101, doi:10.1016/j.msec.2014.05.035.
21. Wang, T.; Ni, G.; Furushima, T.; Diao, H.; Zhang, P.; Chen, S.; Fogarty, C.E.; Jiang, Z.; Liu, X.; Li, H. Mg Alloy Surface Immobilised with Caerin Peptides Acquires Enhanced Antibacterial Ability and Putatively Improved Corrosion Resistance. *Materials Science and Engineering: C* **2021**, *121*, 111819, doi:10.1016/j.msec.2020.111819.
22. Huang, C.H.; Lai, J.J.; Wei, T.Y.; Chen, Y.H.; Wang, X.; Kuan, S.Y.; Huang, J.C. Improvement of Bio-Corrosion Resistance for Ti42Zr40Si15Ta3 Metallic Glasses in Simulated Body Fluid by Annealing within Supercooled Liquid Region. *Materials Science and Engineering: C* **2015**, *52*, 144–150, doi:10.1016/j.msec.2015.03.056.
23. Flux, E.; van der Krogt, M.M.; Cappa, P.; Petrarca, M.; Desloovere, K.; Harlaar, J. The Human Body Model versus Conventional Gait Models for Kinematic Gait Analysis in Children with Cerebral Palsy. *Human Movement Science* **2020**, *70*, 102585, doi:10.1016/j.humov.2020.102585.
24. Pediatric Occupant Human Body Model Kinematic and Kinetic Response Variation to Changes in Seating Posture in Simulated Frontal Impacts – with and without Automatic Emergency Braking. *Traffic Injury Prevention* **2020**, *21*, S49–S53, doi:10.1080/15389588.2020.1825699.

25. Nama, T.; Deb, S. Chapter 12 - Teleportation of Human Body Kinematics for a Tangible Humanoid Robot Control. In *Cognitive Computing for Human-Robot Interaction*; Mittal, M., Shah, R.R., Roy, S., Eds.; Cognitive Data Science in Sustainable Computing; Academic Press, 2021; pp. 231–251 ISBN 978-0-323-85769-7.
26. Pacher, L.; Vignais, N.; Chatellier, C.; Vauzelle, R.; Fradet, L. The Contribution of Multibody Optimization When Using Inertial Measurement Units to Compute Lower-Body Kinematics. *Medical Engineering & Physics* **2023**, *111*, 103927, doi:10.1016/j.medengphy.2022.103927.
27. Eveleigh, K.J.; Deluzio, K.J.; Scott, S.H.; Laende, E.K. Principal Component Analysis of Whole-Body Kinematics Using Markerless Motion Capture during Static Balance Tasks. *Journal of Biomechanics* **2023**, *152*, 111556, doi:10.1016/j.jbiomech.2023.111556.
28. Mashali, M.A.; Saad, N.S.; Canan, B.D.; Elnakish, M.T.; Milani-Nejad, N.; Chung, J.-H.; Schultz, E.J.; Kiduko, S.A.; Huang, A.W.; Hare, A.N.; et al. Impact of Etiology on Force and Kinetics of Left Ventricular End-Stage Failing Human Myocardium. *Journal of Molecular and Cellular Cardiology* **2021**, *156*, 7–19, doi:10.1016/j.yjmcc.2021.03.007.
29. Colavita, F.; Mazzotta, V.; Rozera, G.; Abbate, I.; Carletti, F.; Pinnetti, C.; Matusali, G.; Meschi, S.; Mondi, A.; Lapa, D.; et al. Kinetics of Viral DNA in Body Fluids and Antibody Response in Patients with Acute Monkeypox Virus Infection. *iScience* **2023**, *26*, 106102, doi:10.1016/j.isci.2023.106102.
30. Normand, M.A.; Lee, J.; Su, H.; Sulzer, J.S. The Effect of Hip Exoskeleton Weight on Kinematics, Kinetics, and Electromyography during Human Walking. *Journal of Biomechanics* **2023**, *152*, 111552, doi:10.1016/j.jbiomech.2023.111552.
31. Zernicke, R.; Goulet, G.; Cavanagh, P.; Nigg, B.; JA, A.; HA, M.; van den Bogert, A. Impact of Biomechanics Research on Society. *Kinesiology Reviews* **2011**, *1*, doi:10.1123/krj.1.1.5.
32. Huamanchahua, D.; Vargas-Martinez, A.; Ramirez-Mendoza, R. Kinematic of the Position and Orientation Synchronization of the Posture of a n DoF Upper-Limb Exoskeleton with a Virtual Object in an Immersive Virtual Reality Environment. *Electronics* **2021**, *10*, 1069, doi:10.3390/electronics10091069.
33. Zheng, Y.; Li, L.; Xiang, Y.; He, Y.; Yan, C.; Asano, F. Motion Analysis of Passive Dynamic Walking with a Rigorously Constraint Model: A Necessary Condition for Maintaining Period-1 Gait. *Biomimetic Intelligence and Robotics* **2022**, *2*, 100048, doi:10.1016/j.birob.2022.100048.
34. Ding, M.; Baba, R.; Masanthia, K.; Ricardez, G.A.G.; Takamatsu, J.; Ogasawara, T. Estimation of the Operating Force From the Human Motion. *Annu Int Conf IEEE Eng Med Biol Soc* **2018**, *2018*, 1751–1754, doi:10.1109/EMBC.2018.8512702.
35. Wang, Z.; Yang, C.; Feng, K.; Qin, X. Modeling and Simulation of Musculoskeletal System of Human Lower Limb Based on Tensegrity Structure. *Comput Methods Biomech Biomed Engin* **2019**, *22*, 1282–1293, doi:10.1080/10255842.2019.1661389.
36. Larsen, R.J.; Queen, R.M.; Schmitt, D. Adaptive Locomotion: Foot Strike Pattern and Limb Mechanical Stiffness While Running over an Obstacle. *Journal of Biomechanics* **2022**, *143*, 111283, doi:10.1016/j.jbiomech.2022.111283.
37. Hatamzadeh, M.; Busé, L.; Chorin, F.; Alliez, P.; Favreau, J.-D.; Zory, R. A Kinematic-Geometric Model Based on Ankles' Depth Trajectory in Frontal Plane for Gait Analysis Using a Single RGB-D Camera. *Journal of Biomechanics* **2022**, *145*, 111358, doi:10.1016/j.jbiomech.2022.111358.
38. Ganea, D.; Mereuta, E.; Veresiu, S.; Rus, M.; Amortila, V. Analysis of Reaction Forces in Human Ankle Joint during Gait. In Proceedings of the 21st Innovative Manufacturing Engineering & Energy International Conference - Imane&e 2017; Slatineanu, L., Nagit, G., Dodun, O., Merticaru, V., Coteata, M., Ripanu, M.I., Mihalache, A.M., Boca, M., Ibanescu, R., Panait, C.E., Oancea, G., Kyratsis, P., Eds.; E D P Sciences: Cedex A, 2017; Vol. 112, p. 07019.
39. Karandikar, N.; Ortiz Vargas, O. Kinetic Chains: A Review of the Concept and Its Clinical Applications. *PM & R© : the journal of injury, function, and rehabilitation* **2011**, *3*, 739–745, doi:10.1016/j.pmrj.2011.02.021.
40. Cao, C.-T.; Do, V.-P.; Lee, B.-R. A Novel Indirect Calibration Approach for Robot Positioning Error Compensation Based on Neural Network and Hand-Eye Vision. *Applied Sciences* **2019**, *9*, 1940, doi:10.3390/app9091940.